1521-0103/384/2/254–264$35.00
THE JOURNAL OF PHARMACOLOGY AND EXPERIMENTAL THERAPEUTICS
dx.doi.org/10.1124/jpet.122.001189
J Pharmacol Exp Ther 384:254–264, February 2023

The Journal of PHARMACOLOGY And Experimental Therapeutics

Chlorogenic Acid Inhibits Epithelial-Mesenchymal Transition and Invasion of Breast Cancer by Down-Regulating LRP6[S]

Wei Xue,[1] Jie Hao,[1] Qiuping Zhang,[1] Ronghua Jin, Zhuo Luo, Xin Yang, Yanying Liu, Qinpei Lu, Yiqiang Ouyang, and Hongwei Guo

Guangxi Key Laboratory of Bioactive Molecules Research and Evaluation & College of Pharmacy (W.X., J.H., Q.Z., R.J., Z.L., Y.L., Q.L., H.G.), Key Laboratory of Longevity and Aging-related Diseases of Chinese Ministry of Education & Center for Translational Medicine (W.X, J.H., Q.Z., X.Y., H.G.), and Laboratory Animal Center (Y.O.), Guangxi Medical University, Nanning, China; Department of Pharmacy, Ruikang Hospital Affiliated to Guangxi University of Chinese Medicine, Nanning, China (W.X.); and The First Affiliated Hospital of Guangxi Medical University, Nanning, China (Q.Z.)

Received March 8, 2022; accepted October 17, 2022

ABSTRACT

Epithelial-mesenchymal transition (EMT) is a crucial biologic process for breast cancer metastasis, and inhibition of EMT could be an effective approach to suppress metastatic potential of mammary cancer. High expression of low-density lipoprotein receptor-related protein 6 (LRP6) is usually observed in breast carcinoma and predicts poor prognosis. In the present study, we investigated whether chlorogenic acid (CA) can inhibit the EMT of breast cancer cells and underlying molecular mechanism. We found that CA treatment transformed MCF-7 cell morphology from spindle shape (mesenchymal phenotype) to spherical shape (epithelial phenotype). CA clearly increased epithelial biomarkers' expression (E-cadherin and ZO-1) but decreased mesenchymal proteins' expression (ZEB1, N-cadherin, vimentin, snail, and slug). In addition, CA attenuated MMP-2 and MMP-9 activities and inhibited cell migration and invasion. CA downregulated the expression of LRP6 in MCF-7 cells. Knockdown LRP6 with siRNA repressed cell mobility and invasion, wheras overexpression of LRP6 promoted EMT and antagonized the EMT inhibitory effect of CA on MCF-7 cells. Furthermore, CA directly interacted with Wnt/β-catenin signaling coreceptor LRP6 and reduced LRP6, p-LRP6, and β-catenin expression levels in MCF-7 cells. In vivo study revealed that CA notably reduced tumor volume and tumor weight. CA decreased the expression of LRP6, N-cadherin, ZEB1, vimentin, MMP2, MMP9, and increased the expression of E-cadherin and ZO-1. In conclusion, CA inhibited EMT and invasion of breast cancer by targeting LRP6.

SIGNIFICANCE STATEMENT

CA, the familiar polyphenol compound in traditional Chinese medicine, repressed EMT and weakened cellular mobility and invasion in MCF-7 cells. The mechanism studies demonstrated that CA could inhibit EMT and invasion of MCF-7 cells via targeting LRP6. Additionally, CA restrained tumor growth and xenograft tumor EMT in vivo. The EMT inhibitory property of CA warrants further studies of CA as a drug candidate for the therapy of metastatic breast carcinoma.

Introduction

Breast cancer is the most common cancer in women and has surpassed lung cancer as the most frequently diagnosed tumor, with 2.3 million new cases (11.7%) and 684,996 (6.9%) mammary tumor–related mortalities globally in 2020 (Sung et al., 2021). Although the 5-year relative survival rate for localized breast cancer is relatively high (80%–92%), the 5-year relative survival rate for metastatic breast cancer decreases significantly to <25% (Desantis et al., 2016). Therefore, identification of new treatment of the breast tumor is important.

Epithelial-mesenchymal transition (EMT) is very important in embryonic development (Polyak and Weinberg, 2009). Increasing evidence has shown that EMT also facilitates cancer progression. During the progression of epithelial tumors, EMT participates in the process of seeding metastasis by increasing cell-migrated and invasive capacity (Kalluri and Weinberg, 2009). EMT is induced with an increase of mesenchymal proteins, such as ZEB1, N-cadherin, vimentin, Snail, and Slug, and a decrease of epithelial proteins, including E-cadherin and ZO-1 (Zeisberg and Neilson, 2009). Besides, upregulation of matrix metalloproteinases (MMPs) and fibronectin expression is observed during EMT, which increases cell mobility and invasion (Lee et al., 2006). Since E-cadherin

This work was supported by National Natural Science Foundation of China (82074347), Guangxi key research and development project (GUIKE AB20238004), Innovation Project of Guangxi Graduate Education (YCBZ2021048), and Advanced Innovation Teams and Xinghu Scholars Program of Guangxi Medical University.
The authors declare that they have no competing interests.
[1]W.X., J.H., and Q.Z. contributed equally to this work.
dx.doi.org/10.1124/jpet.122.001189.
This article has supplemental material available at jpet.aspetjournals.org.

ABBREVIATIONS: CA, chlorogenic acid; CST, Cell Signaling Technology; EMT, epithelial-mesenchymal transition; LRP6, low-density lipoprotein receptor–related protein 6; MMP, matrix metalloproteinase; MST, microscale thermophoresis; qRT-PCR, quantitative reverse-transcription polymerase chain reaction; siRNA, small interfering RNA.

is one of the major constituents of the epithelial cell junction system and exerts a potent invasion-inhibiting role in cancer cells, downregulation of E-cadherin occurs in cancer metastasis and always indicates poor prognosis (Comijn et al., 2001). Transcriptional factors, such as ZEB1, Snail, and Slug, play pivotal roles in EMT process induction by suppressing E-cadherin expression and promoting mesenchymal markers' expression (Baritaki et al., 2009; Sun et al., 2012). These biomarker-mediated EMTs are also associated with the mechanism underlying chemoresistance in various kinds of tumors (Gravdal et al., 2007). Thus, developing EMT inhibitors may be an effective way to restrain cancer metastasis.

Chlorogenic acid (CA) is the primary active component of many traditional Chinese herbal medicine and abundant in honeysuckle and *Eucommia ulmoides Oliv* (Miao and Xiang, 2020). Previous studies have shown that CA possesses various pharmacological properties, such as anti-inflammatory (Hwang et al., 2014), antioxidant (Singh et al., 2018), antibiotic (Ren et al., 2015), and anticancer activities (Yang et al., 2021). For instance, Bandyopadhyay et al. (2004) have found that CA represses Bcr-Abl tyrosine kinase and induces p38 MAPK-dependent apoptosis in chronic myelogenous leukemia cells. Yamagata et al. (2018) have reported that CA triggers apoptosis and downregulates stem cell–associated markers' expression in A549 human lung cancer cells. A study by Refolo et al. (2018) has shown that CA enhances regorafenib-mediated cell growth, apoptosis, and cell mobility inhibition in human hepatocellular carcinoma cells. Besides these bioactivities, CA also has a potential inhibitory effect on cancer invasion and metastasis. In hepatoma, CA suppressed the expression of MMP-2 and MMP-9 in HepG2 xenograft tissue (Yan et al., 2017). In prostate cancer, CA significantly lowered the expression of HIF-1, which is associated with cancer metastasis, in hypoxia-induced DU145 cells (Lee et al., 2017). However, whether CA can restrain EMT in breast cancer cell lines is unclear. In this study, we focused on metastatic breast cancer to explore the inhibitory effect and molecular mechanism of CA on EMT.

Materials and Methods

Drug Virtual Screening. The ligand set is created based on the natural-products subset of ZINC15 (https://zinc15.docking.org/). The 3D structure of receptor (low-density lipoprotein receptor-related protein 6, LRP6) is from Uniprot (https://www.uniprot.org/). The interaction domains are predicted by ProDomain with Hmmer domain identification algorithm and IntercDome Ligand-Protein Binding Scoring Algorithm to make the grid setting. Then, the ligand-receptor docking is achieved with Vina. Each ligand has 10 poses binding to the receptor and docking scores (affinity). The sorting rule is based on the affinity. The top 10 small molecules are selected after docking process.

Cell Culture. MCF-7 and MDA-MB-231 cells were purchased from Stem Cell Bank, Chinese Academy of Sciences. Cells were maintained in F-12K medium (Invitrogen, Carlsbad, CA) supplemented with 10% (v/v) FBS (Gibco, Carlsbad, CA) and kept in a 5% CO_2 incubator at 37°C.

CCK-8 Assay. MCF-7 cells were seeded into 96-well plates and cultured overnight. Next, cells were incubated with multiple concentration of CA (25, 12.5, 6.25, 3.125, 1.5625, and 0 μM) for 48 hours. After that, cell growth rate was detected with CCK-8 reagent (Beyotime Biotechnology, Shanghai, China) in accordance with the manufacturer's protocol.

Immunofluorescence Assay. MCF-7 cells were seeded into confocal dishes and incubated with 2.5 μM of CA for 48 hours. Then, cells were fixed with 4% paraformaldehyde for 10 minutes, incubated with 5% bull serum albumin for 1 hour at room temperature, and incubated with primary antibodies against vimentin and E-cadherin (Cell Signaling Technology, Danvers, MA), respectively, overnight at 4°C. The following day, cells were rinsed with PBS and incubated with Alexa Fluor 488 Donkey anti-Rabbit IgG for 1 hour and stained with diamidine phenylindole for 5 minutes at room temperature. Images of fluorescence were acquired by a laser-scanning confocal microscope (LSM 880, ZEISS), and the quantification of fluorescence intensity was processed by using Image-Pro Plus 6.0 software.

Quantitative Reverse-Transcription Polymerase Chain Reaction Assay. Total RNA was extracted from MCF-7 cells with Trizol reagent on the basis of the manufacturer's description (Thermo Fisher Scientific, Waltham, MA). cDNA was produced with Transcriptor First Strand cDNA Synthesis Kit (Roche, Mannheim, Germany). SYBR Green I Master Mix (Roche) and DNA templates were mixed to form the PCR system. Relative expression levels of target genes were determined by the Lightcycler 480 real-time PCR system (Roche). Glyceraldehyde-3-phosphate dehydrogenase was regarded as an internal reference. Primers are displayed in Supplemental Table 1.

Western Blot. Cell pellets were collected and resuspended in RIPA buffer. BCA protein assay kit (Thermo Fisher Scientific) was used to measure the concentration of total protein. Forty micrograms of sample proteins were separated by 8% or 12% SDS-PAGE, then sample proteins were transferred to polyvinylidene difluoride membranes, which were blocked with 5% skim milk for 1 hour at room temperature and incubated with primary antibodies overnight at 4°C. After the membrane was probed with the indicated secondary antibodies for 1 hour at room temperature, membrane images were developed with the enhanced chemiluminescence system (Bio-Rad Clarity Western ECL). β-Actin was the loading control. All antibodies were supplied by Cell Signaling Technology (CST), including EMT Antibody Sampler Kit, MMP-2, MMP-9, LRP6, p-LRP6, β-catenin, β-actin, and horseradish peroxidase–conjugated secondary antibodies.

Gelatin Zymography for Detection of Matrix-Metalloproteinase-2 and -9. Cells were collected and lysed after treatment with 2.5 μM of CA for 48 hours. Sample proteins were quantified, and then diluted with a concentration of 4× sample buffer. Then, 20 μL of sample was loaded into SDS-PAGE gel supplemented with 0.1 mg/mL gelatin. The detection of MMP-2 and MMP-9 was performed with gelatin zymography kit (Wanleibio, Shenyang, China).

Wound-Healing Assay. A scratch wound was generated with a pipette tip, and the degree of wound healing was recorded after 0 and 48 hours, respectively. Images were obtained to evaluate the migratory potential of cells.

Migration and Invasion Assay. Cells were incubated with 2.5 μM of CA for 48 hour and resuspended in no-serum F-12K medium. For migration assay, 2×10^4 cells/100 μL were cultured in transwell inserts (8-μM pore size, Corning Costar, NY). For invasion assay, 2×10^4 cells/100 μL were seeded into transwell inserts coated with Matrigel (BD Biosciences). The 200 μL of no-serum F-12K medium was added to the upper chamber, and the 600 μL of F-12K medium containing 10% FBS was added to the lower chamber. Forty-eight hours later, the upper chambers were taken out and immersed in 4% polyformaldehyde for 30 minutes to fix the cells. Cellular morphology was visualized through staining with 0.1% crystal violet for 30 minutes at room temperature. Cells on the upper membrane of the upper chamber were removed with a cotton bud, and cells that migrated or invaded to the lower surface of the upper chamber were counted under a microscope. The average number of migrating or invasive cells per field was calculated five random fields per membrane.

Cell Transfection. LRP6 small interfering RNA (siRNA) and negative control siRNA were obtained from Beijing Ruibo Xingke Biotechnology Co., Ltd. (Beijing, China). pCMV6-LRP6 and vector pCMV6-Entry were purchased from Origene Technologies Inc. (Rockville, MD). Cells were plated in 6-well plates. When the cell density reached 80%,

indicated plasmids were transfected into cells by using Lipofectamine 3000 (Thermo Fisher Scientific) according to the manufacturer's protocol. Twenty-four hours later, medium containing Lipofectamine 3000 was replaced with fresh medium containing 2.5 μM of CA, and cells were maintained for another 48 hours.

Microscale Thermophoresis. Microscale thermophoresis (MST) was performed to study CA-LRP6 interaction using Monolith NT.115 Microscale Thermophoresis instrument (Nano Temper Technologies, Germany). In brief, LRP6 was labeled with Monolith NT.115 Protein Labeling Kit RED-NHS according to the manufacturer's instructions. CA was serially diluted in PBS with 0.05% Tween-20 to obtain varing concentrations. The binding study was carried using NT.115 premium capillaries, and the assay was performed in triplicates. Data analysis was performed using NTAnalysis software.

Animals and Tumor Formation in Nude Mice. Four- to 6-week-old nu/nu Balb/c mice (female) were supplied by Vital River Laboratory Animal Technology Co. Ltd. (Beijing, China). Animals received humane care according to the guidelines of the Experimental Animal Ethics Committee. Ten million of MCF-7 cells were grafted hypodermically on the back of mice. After the tumor developed to around 100 mm^3, mice were stochastically divided into two groups, including control group and CA group. Mice were treated with normal saline or 10 mg/kg CA through intraperitoneal administration every day. Tumor size was measured with calipers every 3 days, and tumor volume was derived with this formula: $0.5 \times a \times b^2$, where a referred to the long diameter and b to the short diameter of the tumor. Mouse body weight was recorded every three days. Mice were euthanized after 3 weeks, and xenografts were collected, weighed, and soaked in 4% paraformaldehyde for further assays.

Immunohistochemistry Assay. Xenograft tumors were dehydrated, embedded in paraffin, and sliced into 5-μM thickness. Then, these sections were treated with 0.5% TritonX-100 for 30 minutes at room temperature, repaired with 0.01 M sodium citrate buffer solution under microwave, and blocked with 5% bovine serum albumin for 1 hour at room temperature. Next, these sections were incubated with primary antibodies, including anti-rabbit LRP6 antibody (dilution 1:400, CST), anti-rabbit vimentin antibody (dilution 1:200, CST), and anti-rabbit E-cadherin antibody (dilution 1:200, CST), at 4°C overnight, followed by the secondary antibody. Finally, these slices were dyed with a 3,3′-diaminobenzidine tetrahydrochloride kit and observed under a microscope. The integrated optical density values of LRP6, vimentin, and E-cadherin at each visual field (400× magnification) were quantified with the Image-Pro Plus 6.0 software.

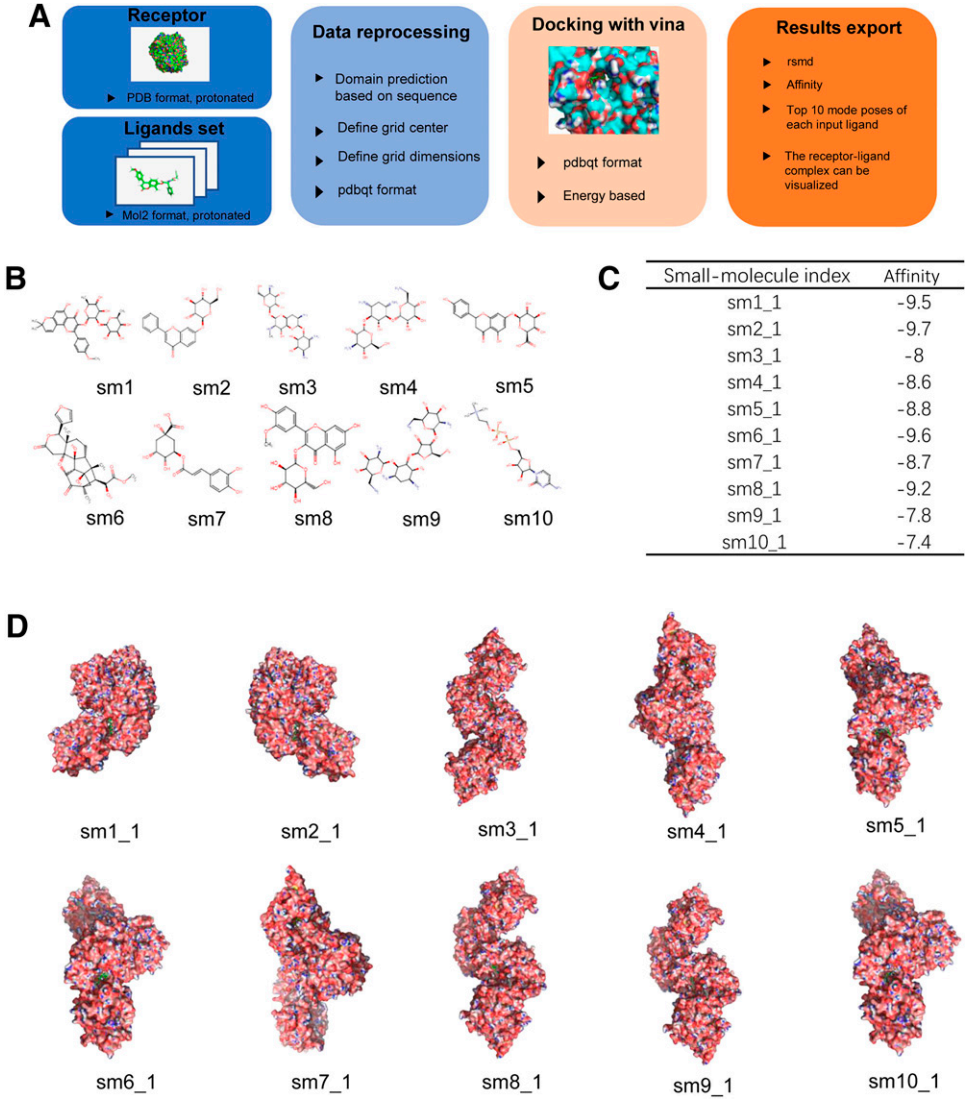

Fig. 1. Virtual screening of small molecules targeting LRP6. (A) The drug virtual screening process based on Vina and ProtDomain. (B) The 2D structures of the selected 10 small molecules. (C) The docking score (affinity) of the selected 10 small molecules with best pose. (D) The binding position and best pose of the selected 10 small molecules.

Statistics. Data are presented as mean ± S.D. Student's *t* test was used to determine whether the difference between the two groups was statistically significant. The statistical differences among three groups were analyzed by one-way analysis of variance. $P < 0.05$ was regarded as the level of significance.

Results

Virtual Screening and Preliminary Identification of Small Molecules Targeting LRP6. We applied Vina and ProtDomain softwares to proceed the drug virtual screening (Fig. 1A). The 2D structures of the selected 10 small molecules are shown in Fig. 1B. The docking score (affinity) of the selected 10 small molecules with best pose to LRP6 is presented in Fig. 1C. The binding position and best pose of the selected 10 small molecules are presented in Fig. 1D. We first detected the nontoxic concentrations of the selected 10 small molecules in MCF-7 cells (Supplemental Table 2). Among them, the small molecule #9 was excluded due to the nonresolve ability. We then used the nontoxic concentration of 6.25 μM to explore their roles in cancer. Morphologic observation was performed under a microscope after cells were administered 6.25 μM of small molecules. Except the small molecular #7 (CA), the morphology of MCF-7 cells treated with other small molecules could not exhibit epithelial cobblestone phenotype (epithelial phenotype) (Supplemental Fig. 1). Therefore, we focused on the CA in our next experiments.

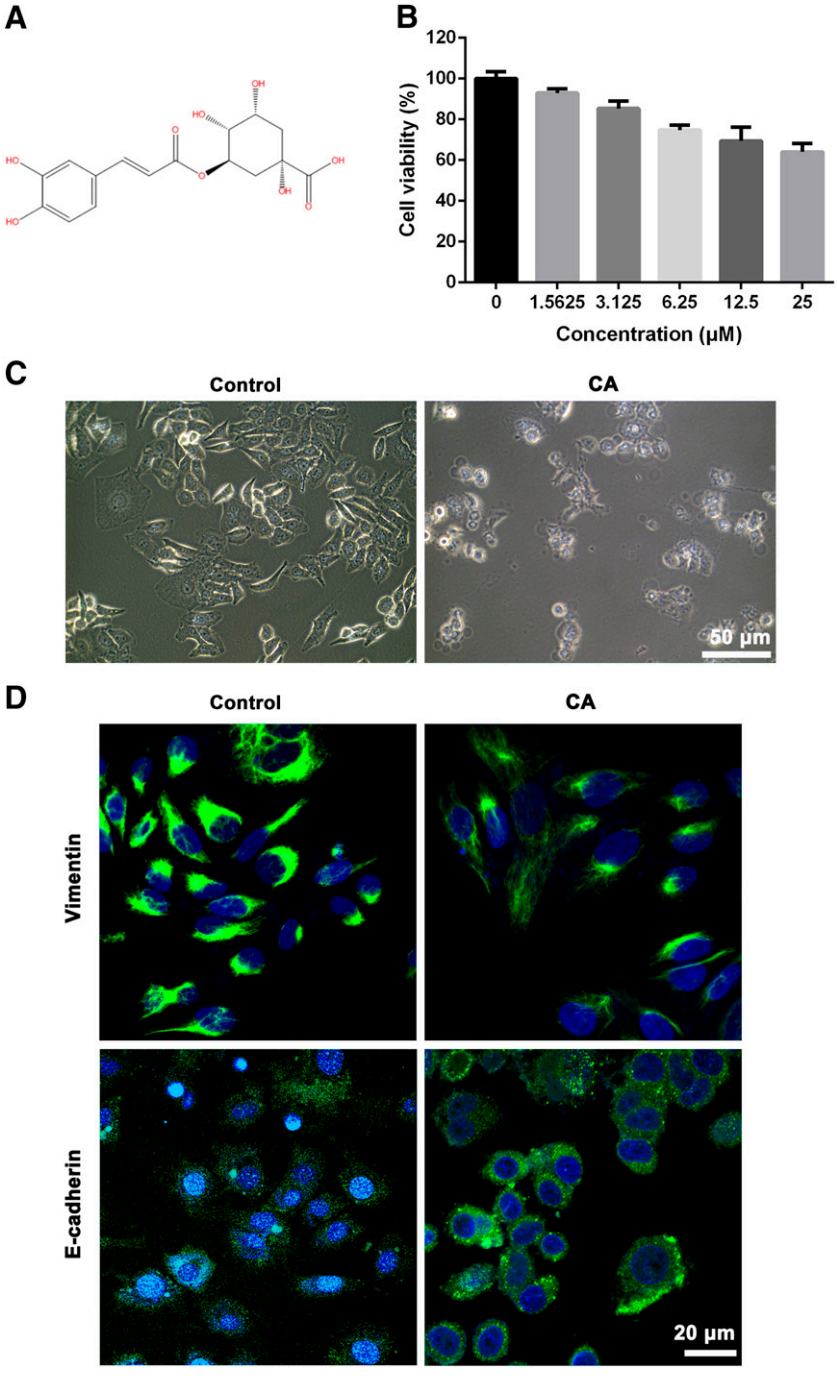

Fig. 2. The morphology of MCF-7 cells converted from a mesenchymal-like type to an epithelial-like type after CA treatment. (A) The chemical structure of CA. (B) After treatment with various concentrations of CA for 48 hours, the viability of MCF-7 cells was measured with a CCK-8 assay. (C) After 48 hours of incubation with 2.5 μM of CA, the shape of MCF-7 cells was captured using a microscope (scale bar, 50 μM). (D) Vimentin and E-cadherin were detected by immunofluorescent staining in MCF-7 cells after CA treatment of 48 hours (scale bar, 20 μM). Data are expressed as the mean ± S.D. ($n = 3$).

CA Changed the Morphology of MCF-7 Cells from a Mesenchymal Morphology to an Epithelial Morphology. The chemical structure of CA is shown in Fig. 2A. Since this study focuses on the inhibitory effect of CA on EMT, we further detected the nontoxic concentrations of CA (cell viability ≥90%) to exclude the apoptosis effect in breast cancer cell line. As shown in Fig. 2B, the cell viability rate of 90% corresponds to a dose of 2.5 μM. Acquisition of a spindle-shaped morphology, decrease of E-cadherin, and elevated vimentin are hallmarks of mesenchymal phenotypic conversion of epithelia in tumor migration and invasion. Therefore, morphologic observation was performed under a microscope after cells were dosed with 2.5 μM of CA. As displayed in Fig. 2C, the cell morphology in control group was elongated fibroblastic phenotype (mesenchymal phenotype), but the morphology of MCF-7 cells treated with CA exhibited epithelial cobblestone phenotype (epithelial phenotype). Immunofluorescence assay showed that the expression of vimentin decreased and E-cadherin increased after CA treatment (Fig. 2D), indicating that CA has an inhibitory effect on MCF-7 cells EMT.

CA Lowered Mesenchymal Biomarkers' Expression and Elevated Epithelial Proteins' Expression in MCF-7 Cells. To further verify the inhibitory effect on EMT by CA, the mRNA level and protein expression of EMT-related markers, including ZO-1, E-cadherin, N-cadherin, ZEB1, vimentin, Snail, and Slug, were determined in MCF-7 cells. As shown in Fig. 3A, the mRNA level of epithelial markers (ZO-1 and E-cadherin) was elevated after CA treatment, whereas mesenchymal biomarkers' expression (N-cadherin, ZEB1, vimentin, Snail, and Slug) was reduced by CA. Western blot assay showed a similar result. The expression of ZO-1 and E-cadherin was upregulated, whereas N-cadherin, ZEB1, vimentin, Snail, and Slug expression were downregulated after MCF-7 cells were dosed with 2.5 μM of CA (Fig. 3, B and C). We also examined the antagonistic effect of CA on EMT in MDA-MB-231 cells using western blot assay. As shown in Supplemental Fig. 2, the epithelial markers E-cadherin and ZO-1 were upregulated, whereas the mesenchymal markers, such as N-cadherin, ZEB1, vimentin, Snail, and Slug, were downregulated. However, in our further study, we found that CA had no effect on the expression level of LRP6. So, CA can inhibit EMT, but dose not decrease the expression of LRP6 in MDA-MB-231 cells.

CA Repressed the Migratory and Invasive Ability of MCF-7 Cells. MMPs, including MMP-2 and MMP-9, play an important part in cancer invasion by degrading the extracellular matrix. The gelatin zymography assay demonstrated that the activities of MMP-2 and MMP-9 were degraded by CA (Fig. 4, A and B). The expression of MMP-2 and MMP-9 was also decreased by CA (Fig. 4, C and D). A wound-healing experiment was applied to determine the migration potential of MCF-7 cells. Results showed that CA significantly repressed wound closure (Fig. 4, E and F). Cell migration was also examined using a transwell assay with noncoated membrane, and cell invasion was evaluated through a transwell assay with coated membrane. We found that CA markedly attenuated the cellular migration and invasion through the membrane (Fig. 4, G and H). These data indicate that CA can effectively restrain the migration and invasion of MCF-7 cells.

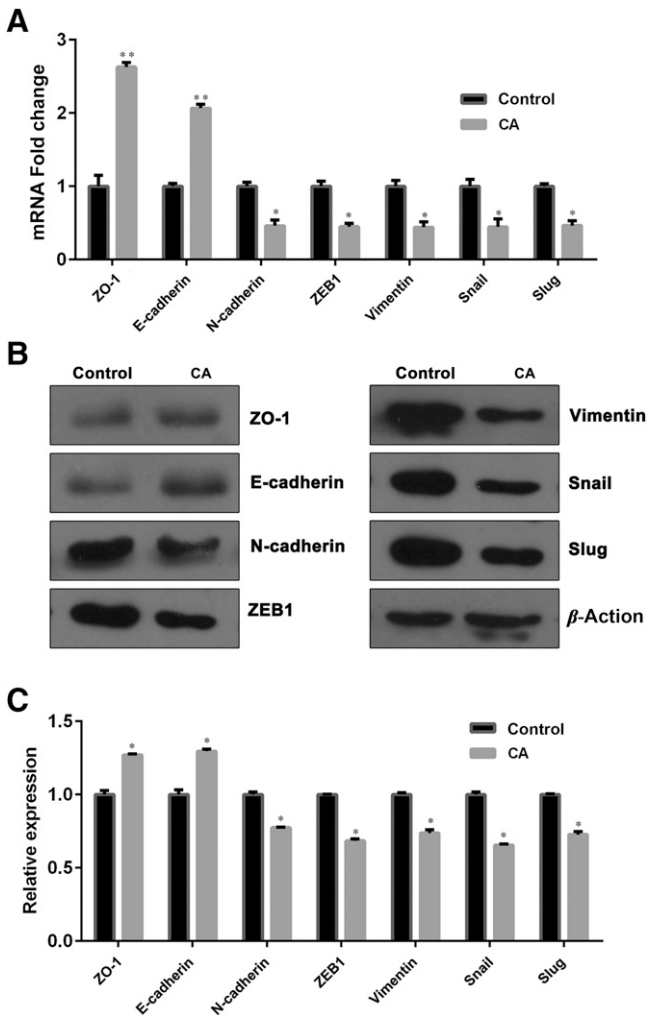

Fig. 3. CA inhibited EMT in MCF-7 cells. MCF-7 cells were administered 2.5 μM of CA for 48 hours, and the expression levels of EMT-related markers were detected. (A) The expression of epithelial markers (ZO-1 and E-cadherin) and mesenchymal markers (N-cadherin, ZEB1, vimentin, Snail, and Slug) was evaluated by qRT-PCR assay (B) and western blot experiment. (C) The relative protein level of EMT markers was quantified using the densitometric analysis. β-Actin was considered an internal control. Results are shown as the mean ± S.D. ($n = 3$). *$P < 0.05$; **$P < 0.01$ versus the control group.

Silencing LRP6 Expression Inhibited Migration, Invasion, and EMT in MCF-7 Cells. As LRP6 has been proven to play a significant role in tumor metastasis, we then examined the effect of CA on LRP6. Quantitative reverse-transcription polymerase chain reaction (qRT-PCR) and western blot assay have shown that the mRNA and protein expression was reduced after CA treatment (Fig. 5, A–C). To elucidate whether LRP6 promotes MCF-7 cell EMT, we developed siRNA interference sequences (LRP6 siRNA) to silence LRP6 expression in MCF-7 cells. The LRP6 siRNA notably decreased both mRNA and protein expression of LRP6 (Fig. 5, D–F). Next, we assessed the effect of LRP6 on MCF-7 cell EMT. Compared with the negative control group, E-cadherin and vimentin expression in MCF-7 cells treated with LRP6 siRNA were observably increased and decreased, respectively. However, compared with the LRP6 siRNA group, knockdown of LRP6 did not enhanced the inhibitory effect of CA on EMT (Fig. 5, G and H). A transwell assay

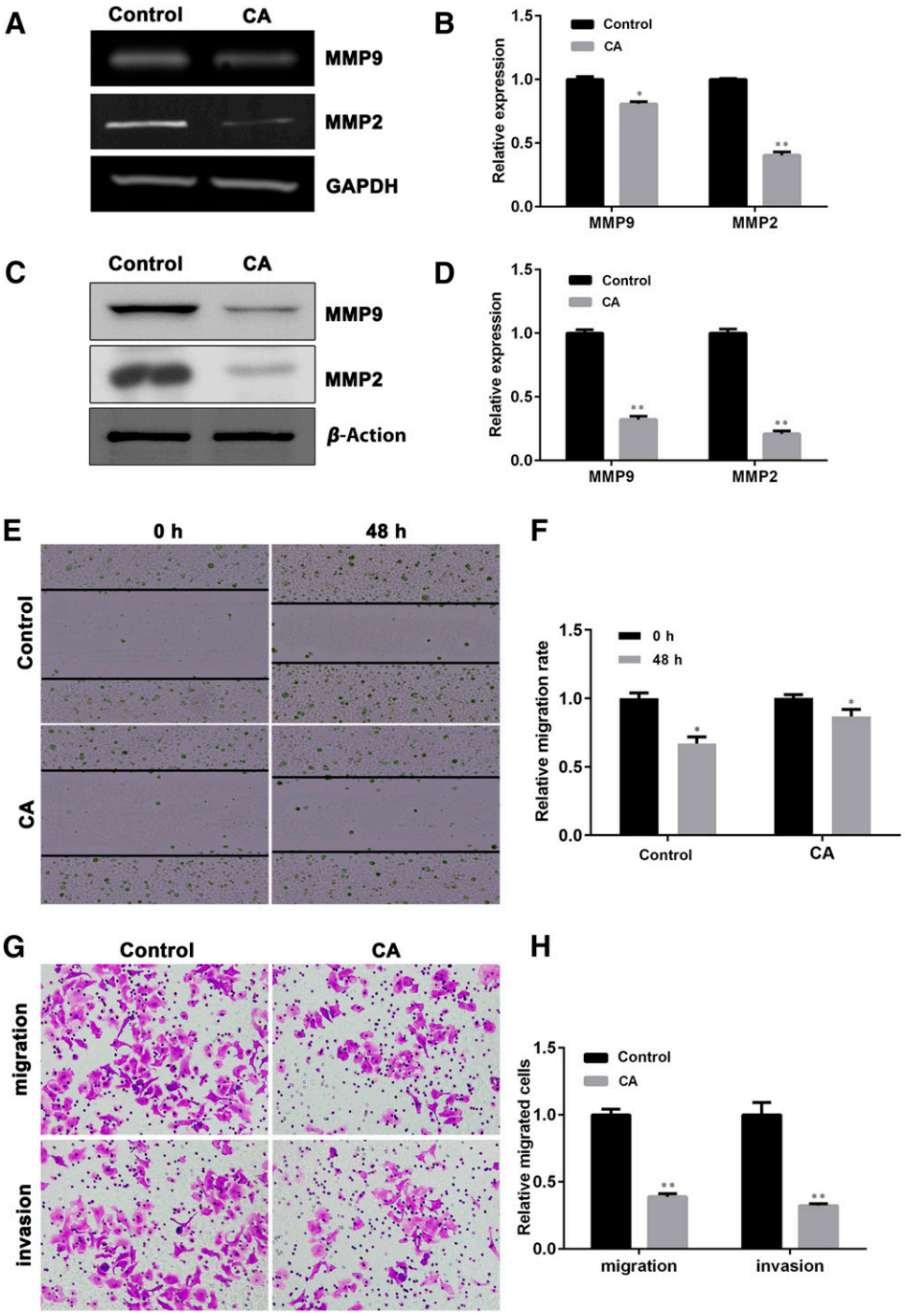

Fig. 4. CA weakened cell migration and invasion. MCF-7 cells were incubated with 2.5 μM of CA for 48 hours. (A) Activities of MMP-2 and MMP-9 degrading extracellular matrix were assessed with gelatin zymography assay. (B) Relative activity was quantified. (C) The expression levels of MMP-2 and MMP-9 were determined by western blot assay. (D) Relative protein expression was quantified. (E) Cell migration potential was detected with a wound-healing experiment. (F) The relative wound width. (G) A transwell assay with noncoated membrane or Matrigel-coated membrane was applied to evaluate cellular migratory and invasive abilities. (H) The relative number of migrated and invasive cells was counted by using Image-Pro Plus. Results are represented as the mean ± S.D. ($n = 3$). *$P<$ 0.05; **$P<$ 0.01 versus the control group.

showed that LRP6 siRNA clearly attenuated cell migration and invasion (Fig. 5, I and J). The above studies suggest that LRP6 promotes breast cancer EMT, and LRP6 may be a potential target of CA to inhibit the EMT in breast cancer.

CA Reversed EMT by Downregulating LRP6 in MCF-7 Cells. Whether CA inhibited MCF-7 cell EMT through repressing LRP6 expression remains unknown. Thus, we constructed LRP6-overexpressed plasmids to determine if overexpression of LRP6 antagonizes the EMT inhibition effect of CA. After MCF-7 cells were transfected with LRP6-overexpressed plasmids, both mRNA and protein levels of LRP6 were markedly augmented (Fig. 6, A–C). Compared with cells transfected with vector, LRP6 overexpression notably reduced E-cadherin expression and upregulated vimentin. However, compared with the LRP6 overexpression group, E-cadherin and vimentin expression was enhanced and reduced, respectively, in cells treated with CA and LRP6-overexpressed plasmids (Fig. 6, D and E). A transwell migration and invasion assay showed similar results. The elevated migration and invasion capacity of MCF-7 cells induced by LRP6 overexpression was diminished by CA (Fig. 6, F and G). These data suggest that CA reversed breast cancer–cell EMT via inhibiting LRP6.

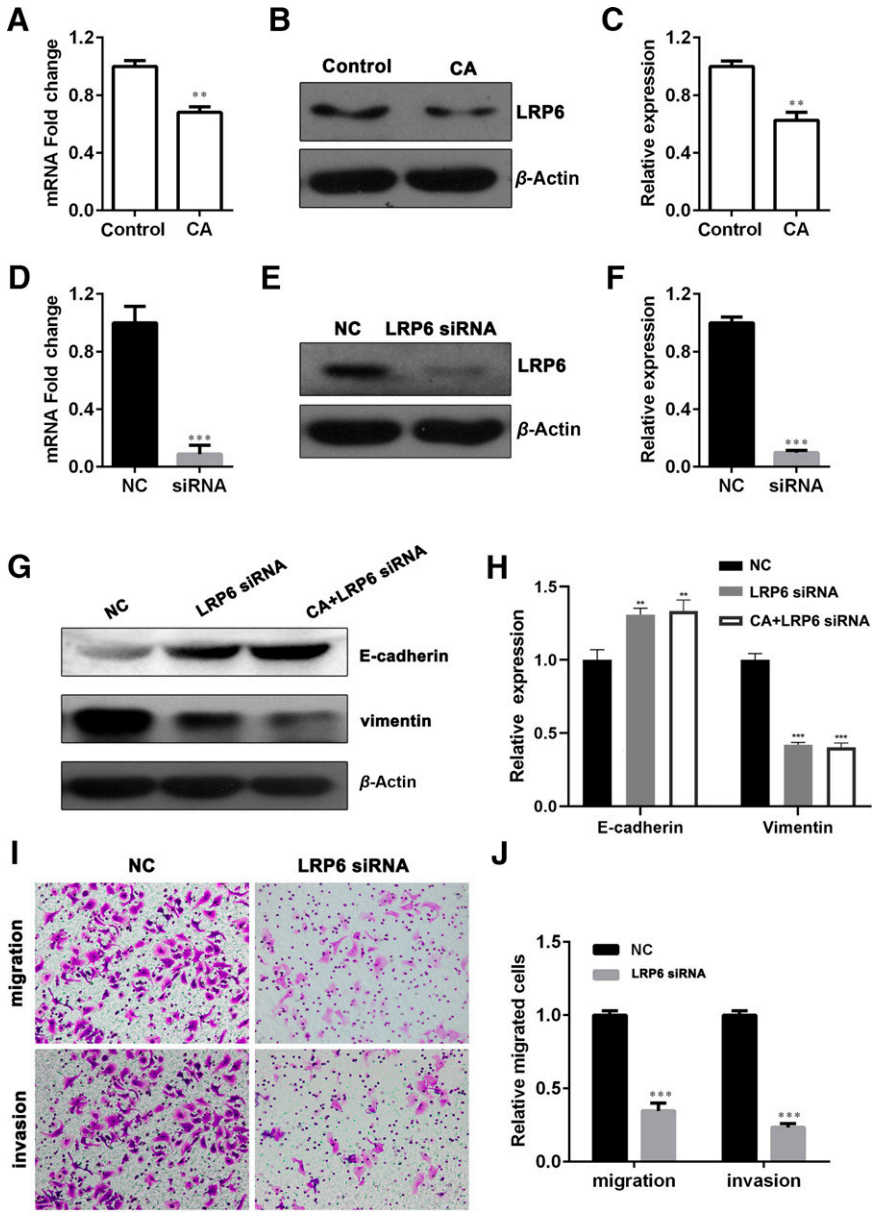

Fig. 5. Silencing LRP6 expression inhibited migration, invasion, and EMT in MCF-7 cells. (A) MCF-7 cells were treated with 2.5 μM of CA for 48 hours, and the mRNA level of LRP6 was determined by qRT-PCR. (B) The protein level of LRP6 was detected by western blot assay. (C) Relative expression of LRP6 was quantified. (D) Transfection of LRP6 siRNA was performed on MCF-7 cells. The mRNA level of LRP6 was examined by qRT-PCR assay. (E) The protein level of LRP6 was detected by the western blot experiment. (F) Relative expression of LRP6 was quantified. (G) The effect of silencing LRP6 on EMT-related markers was determined by western blot experiment. (H) Relative expression of EMT-related markers was quantified. (I) The effect of silencing LRP6 on cell migration and invasion was measured by transwell assay. (J) The relative amount of migrated and invasive cells was counted by using Image-Pro Plus. Statistics are expressed as the mean ± S.D. ($n = 3$). *$P < 0.05$; **$P < 0.01$; ***$P < 0.001$ against the control group. NC, negative control.

CA Directly Binds to LRP6-Inhibited EMT via Wnt/β-Catenin Signaling. To investigate the equilibrium binding constant between CA and LRP6 under close-to-native condition, we performed MST to detect the interaction and the binding affinity. With the MST fit curve, obtained dissociation constant of 2.47 ± 0.45 μM presented strong binding of CA to LRP6 (Fig. 7A). These results indicated that CA may directly bind to LRP6. In addition, LRP6 is a coreceptor of Wnt/β-catenin signaling. To further determine if CA decreased LRP6 expression and inhibited EMT through Wnt/β-catenin signaling in MCF-7 cells, we investigated the levels of LRP6, p-LRP6 (Ser 1490), and β-catenin by western blot. The results showed that CA suppressed the levels of LRP6, p-LRP6 (Ser 1490), and β-catenin in MCF-7 cells (Fig. 7B).

CA Restrained the Growth and EMT of Xenograft Tumors. To further investigate the inhibitory effect of CA in EMT and metastasis in vivo, MCF-7 cells were inoculated into nude mice. After 3 weeks of continuous administration, tumor volume and weight were observably reduced by CA (Fig. 8, A and B; Supplemental Fig. 3). No obvious difference in body weight was observed between the control group and the CA-administered group (Fig. 8C). Immunohistochemistry analysis revealed that the expression of LRP6 and vimentin was lower in the CA-treated group, whereas E-cadherin expression was higher than that in the control group (Fig. 8, D and E). Western blot analysis of in vivo samples also showed that the expression of E-cadherin and ZO-1 were upregulated, whereas LRP6, N-cadherin, ZEB1, vimentin, MMP9, and MMP2 were downregulated (Fig. 8F). These results suggested that CA significantly suppressed LRP6 expression and inhibited EMT in vivo.

Discussion

EMT facilitates cancer metastasis and cancer progression. During EMT seeding metastasis, it not only delivers cancer cells from one organ to another to proliferate but also endows

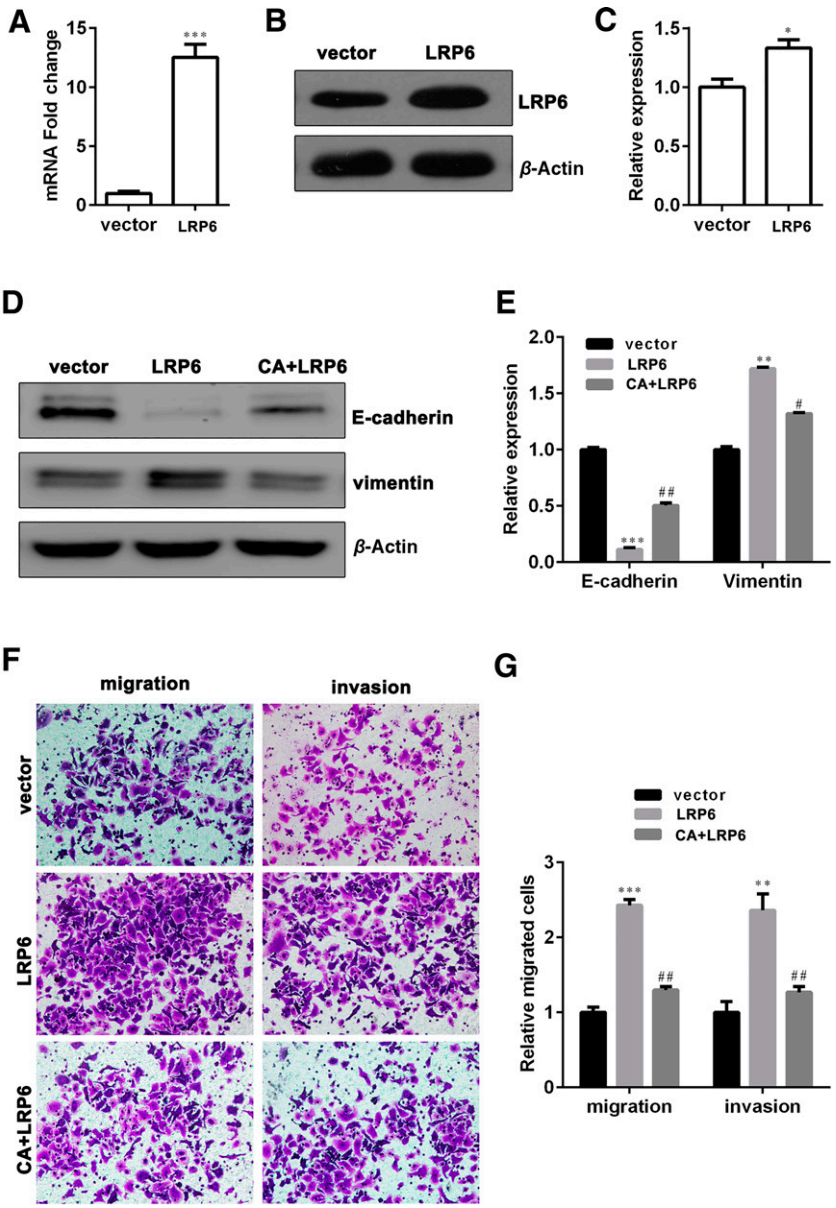

Fig. 6. CA reversed EMT by downregulating LRP6 in MCF-7 cells. MCF-7 cells were transfected with LRP6-overexpressed plasmids. (A) qRT-PCR assay was used to assess the mRNA expression of LRP6. (B) The expression of LRP6 at protein level was determined by western blot assay. (C) Relative expression of LRP6 was quantified. (D) MCF-7 cells were transfected with LRP6-overexpressed plasmids for 24 hours, and then cells were exposed to 2.5 μM of CA for 48 hours. EMT-related markers were evaluated by western blot assay. (E) Relative expression of EMT-related biomarkers was quantified. (F) The effect of LRP6 overexpression on CA-inhibited migration and invasion was assessed by transwell assay. (G) The relative amount of migrated and invasive cells was calculated by using Image-Pro Plus 6.0. Data are shown as the mean ± S.D. (n = 3). $^{*}P< 0.05$; $^{**}P< 0.01$; $^{***}P< 0.001$ against the control group. $^{\#}P< 0.05$; $^{\#\#}P< 0.01$ relative to the LRP6 group.

cancer cells stemness traits, which contributes to the chemotherapy resistance of cancer. Cancer metastasis induced by EMT can enhance malignant and refractory extent, indicating that EMT is closely associated with clinical cancer grade (Cai et al., 2018). Thus, inhibiting EMT could be a doable treatment means for metastatic cancer treatment.

Increasing evidence has testified that CA has an anti-invasive effect on a variety of cancers. In hepatocellular carcinoma, CA has been proven to be one of the chemical entities in coffee inhibiting hepatoma invasion in vitro (Yagasaki et al., 2000). Jin et al. (2005) found that CA strongly inhibited MMP-9 activity in a content-dependent way on zymography in Hep3B cells. Yan et al. (2017) have shown that CA inhibited the growth of HepG2 cells in vitro, decreased MMP-2 and MMP-9 expression in xenograft tumors, and attenuated the progression of HepG2 xenograft in vivo (Liu et al., 2020). In glioma, Belkaid et al. (2006) found that CA represses U-87 glioma cell migration and MMP-2 secretion via inhibiting glucose-6-phosphate translocase (G6PT), whose expression is high in U-87 glioma cells. In breast cancer, Zhang et al. (2015) have proven that a combination of lapatinib and CA can efficaciously restrain macrophage M2 polarization and metastasis of mammary tumors. Yu et al. (2018) pointed out that a derivative of CA, isochlorogenic acid C, isolated from *Lonicera japonica*, reversed EMT via inactivating the EGFR signaling pathway in MDA-MB-231 cells. In fibrosarcoma, Hwang et al. (2010) reported that a derivative of CA, 3-Caffeoyl, 4-dihydrocaffeoylquinic acid (CDCQ), extracted from *Salicornia herbacea*, had anti-invasive effects on human fibrosarcoma HT-1080 cells, and the underlying molecular mechanism was that CDCQ downregulated MMP-9 by inhibiting AP-1 and signaling pathways involving PKC δ and three MAPKs. In present study, we found that CA significantly increased E-cadherin and ZO-1 expression (epithelial markers) and decreased N-cadherin, ZEB1, vimentin, Snail, and Slug expression (mesenchymal markers). In addition, CA downregulated MMP-2 and MMP-9 activities and weakened migration and

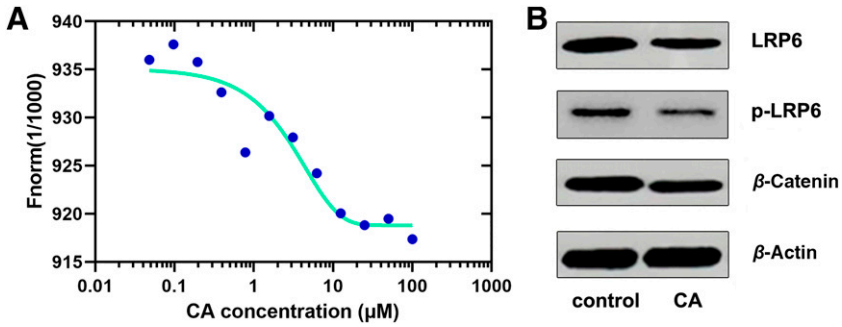

Fig. 7. CA directly binding to LRP6 inhibited the EMT via Wnt/β-catenin signaling in MCF-7 cells. (A) Interaction of CA and LRP6 determined by microscale thermophoresis. (B) Wnt/β-catenin signaling–related proteins were evaluated by western blot assay.

invasion abilities of MCF-7 cells, which indicated that CA has an inhibitory effect on breast cancer EMT. However, the dosage of CA applied in this study differs from previous studies, suggesting that different cancer cell lines have different sensitivities to CA. As far as we know, this study is the first to report that CA can inhibit EMT in breast cancer.

A growing body of evidence in the literature strongly suggests the function of LRP6 in tumorigenesis of breast cancer.

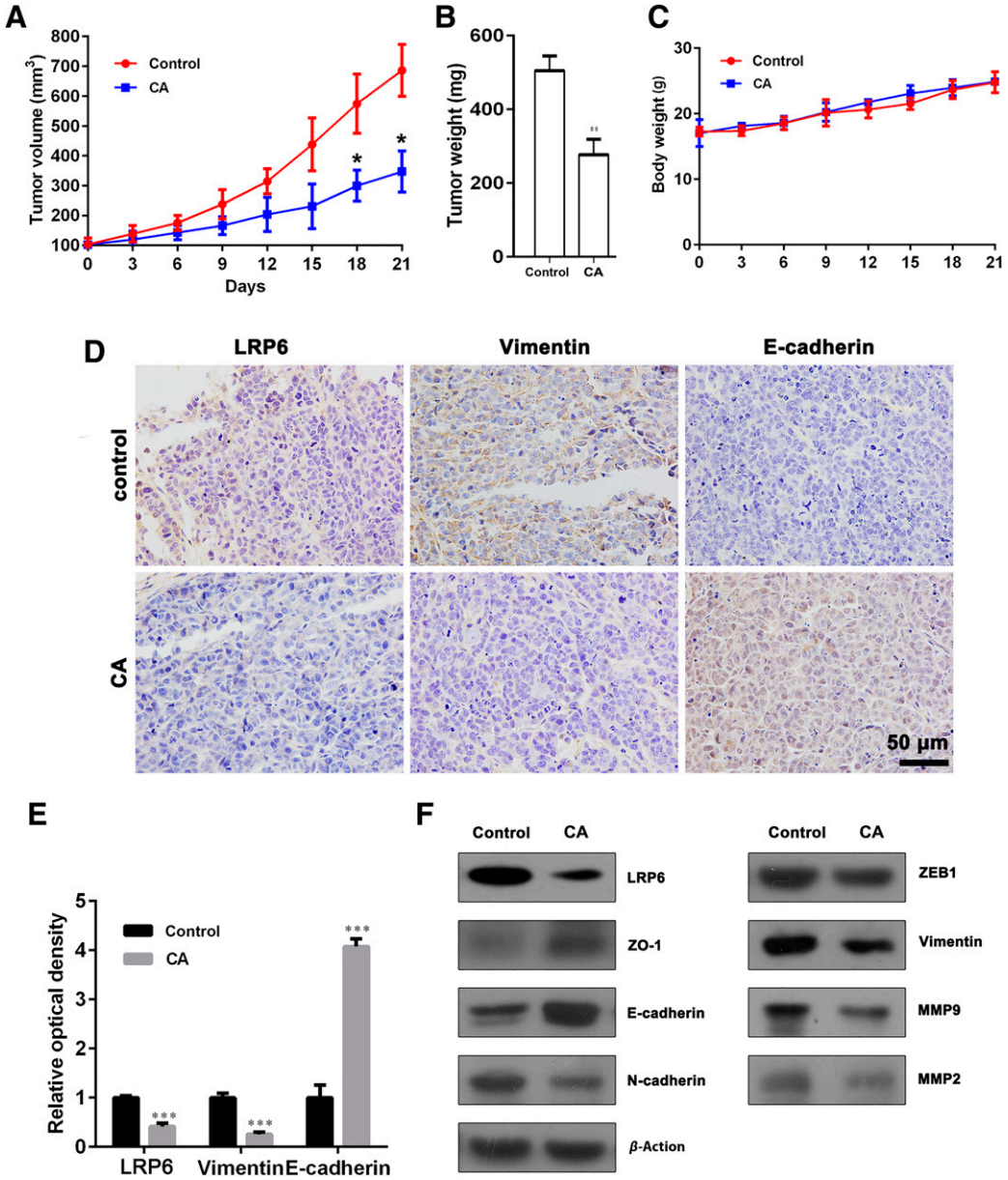

Fig. 8. CA restrained the growth and EMT of xenograft tumors. Nude mice bearing xenograft tumors derived from MCF-7 cells (n = 4 per group) were administered normal saline or 10 mg/kg CA for 3 weeks. (A) Tumor volume, (B) tumor weight, and (C) body weight were shown. (D) Immunohistochemical staining of LRP6, vimentin, and E-cadherin were performed in xenograft tumor tissues (scale bar, 50 μM). (E) Relative expression of LRP6, vimentin, and E-cadherin was quantified. (F) The expression of LRP6, epithelial markers (ZO-1 and E-cadherin), and mesenchymal markers (N-cadherin, ZEB1, vimentin, MMP2, and MMP9) was evaluated by western blot experiment. Data are presented as the mean ± S.D. (n = 3). *P< 0.01; ***P< 0.001 against the control group.

Liu et al. (2010) showed that the expression of LRP6 was increased in a subpopulation of human breast cancers. LRP6 silencing in mammary tumor cells reduced cell growth rate and tumor growth in vivo. An LRP6 antagonist, Mesd, can observably inhibit the growth of MMTV-Wnt1 cancer and has negligible side effects (Liu et al., 2010). Zhang et al. (2010) found that the expression of LRP6 was upregulated in a subset of human breast cancer tissues and cell lines. They found that mammary tissues from MMTV-LRP6 mice exhibited noteworthy Wnt activation, as verified by the transposition of β-catenin from membrane to cytoplasmic/nuclear compartment. Higher expression of multiple Wnt target genes such as Axin2, Cyclin D1, and c-Myc was also found in MMTV-LRP6 mice. Furthermore, compared with wild-type mice, the breast glands of virgin MMTV-LRP6 mice showed marked hyperplasia, a sign of developing breast carcinoma. The expression of some matrix metalloproteinases is increased in MMTV-LRP6 mice, possibly conducive to the proliferative phenotype. Their results indicated that activation of Wnt signaling at the level of cell surface receptors can promote breast cancer development (Zhang et al., 2010). Prodigiosin, a natural red pigment generated by a variety of bacteria, could inactivate the Wnt/β-catenin pathway through blocking the phosphorylation of LRP6 in breast cancer cells. (Wang et al., 2016). Silibinin was shown to inhibit the Wnt/β-catenin pathway through decreasing the Wnt coreceptor LRP6 level in human prostate and breast tumor cells (Lu et al., 2012).

In this study, we found that CA downregulated the mRNA and protein level of LRP6, and knockdown of LRP6 with siRNA interference sequences significantly reversed EMT and attenuated cell migration and invasive capacity, indicating that LRP6 plays a key role in breast carcinoma EMT. Further mechanism study showed that overexpression of LRP6 weakened the EMT inhibitory effect induced by CA, whereas knockdown of LRP6 did not enhance the inhibitory effect of CA on EMT, suggesting that CA represses the EMT of MCF-7 cells via inhibiting LRP6 expression. LRP6 is a coreceptor of Wnt/β-catenin signaling; our experiments have demonstrated that CA directly targeting LRP6 inhibits EMT in breast cancer through Wnt/β-catenin signaling. Previous studies showed that TGF-β and Notch1 pathways play important roles in tumor metastasis (Sulaiman et al., 2021; Zhang et al., 2021). CA decreased expression of LRP6 but did not affect the expression of TGF-β and Notch1 (Supplemental Fig. 4), suggesting that CA targeted to LRP6 through Wnt/β-catenin signaling but not via TGF-β and Notch1 signaling. Moreover, CA could inhibit tumor growth and xenograft tumor EMT in vivo. CA has a good therapeutic effect and is expected to be a potential drug for the treatment of metastatic breast cancer.

In summary, CA can inhibit EMT in breast cancer through downregulating LRP6 expression in vitro and in vivo. CA could be developed as a potential EMT inhibitor for breast cancer treatment. In the future, an orthotopic breast cancer model should be developed, and living animal imaging should be used to monitor tumor metastasis in vivo. Based on the orthotopic breast cancer model, the metastatic activity of CA can be assessed specifically.

Authorship Contributions

Participated in research design: Lu, Ouyang, Guo.
Conducted experiments: Xue, Hao, Zhang, Liu.
Contributed new reagents or analytic tools: Guo.
Performed data analysis: Jin, Luo, Yang.
Contributed to the writing of the manuscript: Xue, Lu.

References

Bandyopadhyay G, Biswas T, Roy KC, Mandal S, Mandal C, Pal BC, Bhattacharya S, Rakshit S, Bhattacharya DK, Chaudhuri U, et al. (2004) Chlorogenic acid inhibits Bcr-Abl tyrosine kinase and triggers p38 mitogen-activated protein kinase-dependent apoptosis in chronic myelogenous leukemic cells. *Blood* **104**:2514–2522.

Baritaki S, Yeung K, Palladino M, Berenson J, and Bonavida B (2009) Pivotal roles of snail inhibition and RKIP induction by the proteasome inhibitor NPI-0052 in tumor cell chemoimmunosensitization. *Cancer Res* **69**:8376–8385.

Belkaid A, Currie JC, Desgagnés J, and Annabi B (2006) The chemopreventive properties of chlorogenic acid reveal a potential new role for the microsomal glucose-6-phosphate translocase in brain tumor progression. *Cancer Cell Int* **6**:7.

Cai Z, Cao Y, Luo Y, Hu H, and Ling H (2018) Signalling mechanism(s) of epithelial-mesenchymal transition and cancer stem cells in tumour therapeutic resistance. *Clin Chim Acta* **483**:156–163.

Comijn J, Berx G, Vermassen P, Verschueren K, van Grunsven L, Bruyneel E, Mareel M, Huylebroeck D, and van Roy F (2001) The two-handed E box binding zinc finger protein SIP1 downregulates E-cadherin and induces invasion. *Mol Cell* **7**:1267–1278.

DeSantis CE, Fedewa SA, Goding Sauer A, Kramer JL, Smith RA, and Jemal A (2016) Breast cancer statistics, 2015: Convergence of incidence rates between black and white women. *CA Cancer J Clin* **66**:31–42.

Gravdal K, Halvorsen OJ, Haukaas SA, and Akslen LA (2007) A switch from E-cadherin to N-cadherin expression indicates epithelial to mesenchymal transition and is of strong and independent importance for the progress of prostate cancer. *Clin Cancer Res* **13**:7003–7011.

Hwang SJ, Kim YW, Park Y, Lee HJ, and Kim KW (2014) Anti-inflammatory effects of chlorogenic acid in lipopolysaccharide-stimulated RAW 264.7 cells. *Inflamm Res* **63**:81–90.

Hwang YP, Yun HJ, Choi JH, Chun HK, Chung YC, Kim SK, Kim BH, Kwon KI, Jeong TC, Lee KY, et al. (2010) 3-Caffeoyl, 4-dihydrocaffeoylquinic acid from Salicornia herbacea inhibits tumor cell invasion by regulating protein kinase C-δ-dependent matrix metalloproteinase-9 expression. *Toxicol Lett* **198**:200–209.

Jin UH, Lee JY, Kang SK, Kim JK, Park WH, Kim JG, Moon SK, and Kim CH (2005) A phenolic compound, 5-caffeoylquinic acid (chlorogenic acid), is a new type and strong matrix metalloproteinase-9 inhibitor: isolation and identification from methanol extract of Euonymus alatus. *Life Sci* **77**:2760–2769.

Kalluri R and Weinberg RA (2009) The basics of epithelial-mesenchymal transition. *J Clin Invest* **119**:1420–1428.

Lee JM, Dedhar S, Kalluri R, and Thompson EW (2006) The epithelial-mesenchymal transition: new insights in signaling, development, and disease. *J Cell Biol* **172**:973–981.

Lee MS, Lee SO, Kim KR, and Lee HJ (2017) Sphingosine Kinase-1 Involves the Inhibitory Action of HIF-1α by Chlorogenic Acid in Hypoxic DU145 Cells. *Int J Mol Sci* **18**:325.

Liu CC, Prior J, Piwnica-Worms D, and Bu G (2010) LRP6 overexpression defines a class of breast cancer subtype and is a target for therapy. *Proc Natl Acad Sci USA* **107**:5136–5141.

Liu Y, Feng Y, Li Y, Hu Y, Zhang Q, Huang Y, Shi K, Ran C, Hou J, Zhou G, et al. (2020) Chlorogenic Acid Decreases Malignant Characteristics of Hepatocellular Carcinoma Cells by Inhibiting DNMT1 Expression. *Front Pharmacol* **11**:867.

Lu W, Lin C, King TD, Chen H, Reynolds RC, and Li Y (2012) Silibinin inhibits Wnt/β-catenin signaling by suppressing Wnt co-receptor LRP6 expression in human prostate and breast cancer cells. *Cell Signal* **24**:2291–2296.

Miao M and Xiang L (2020) Pharmacological action and potential targets of chlorogenic acid. *Adv Pharmacol* **87**:71–88.

Polyak K and Weinberg RA (2009) Transitions between epithelial and mesenchymal states: acquisition of malignant and stem cell traits. *Nat Rev Cancer* **9**:265–273.

Refolo MG, Lippolis C, Carella N, Cavallini A, Messa C, and D'Alessandro R (2018) Chlorogenic acid improves the regorafenib effects in human hepatocellular carcinoma cells. *Int J Mol Sci* **19**:1518–1533.

Ren S, Wu M, Guo J, Zhang W, Liu X, Sun L Holyst R, Hou S, Fang Y, and Feng X (2015) Sterilization of polydimethylsiloxane surface with Chinese herb extract: a new antibiotic mechanism of chlorogenic acid. *Sci Rep* **5**:10464.

Singh SS, Rai SN, Birla H, Zahra W, Kumar G, Gedda MR, Tiwari N, Patnaik R, Singh RK, and Singh SP (2018) Effect of Chlorogenic Acid Supplementation in MPTP-Intoxicated Mouse. *Front Pharmacol* **9**:757.

Sulaiman A, McGarry S, Chilumula SC, Kandunuri R, and Vinod V (2021) Clinically Translatable Approaches of Inhibiting TGF- β to Target Cancer Stem Cells in TNBC. *Biomedicines* **9**:1386.

Sun Y, Wang BE, Leong KG, Yue P, Li L, Jhunjhunwala S, Chen D, Seo K, Modrusan Z, Gao WQ, et al. (2012) Androgen deprivation causes epithelial-mesenchymal transition in the prostate: implications for androgen-deprivation therapy. *Cancer Res* **72**:527–536.

Sung H, Ferlay J, Siegel RL, Laversanne M, Soerjomataram I, Jemal A, and Bray F (2021) Global Cancer Statistics 2020: GLOBOCAN Estimates of Incidence and Mortality Worldwide for 36 Cancers in 185 Countries. *CA Cancer J Clin* **71**:209–249.

Wang Z, Li B, Zhou L, Yu S, Su Z, Song J, Sun Q, Sha O, Wang X, Jiang W, et al. (2016) Prodigiosin inhibits Wnt/β-catenin signaling and exerts anticancer activity in breast cancer cells. *Proc Natl Acad Sci USA* **113**:13150–13155.

Yagasaki K, Miura Y, Okauchi R, and Furuse T (2000) Inhibitory effects of chlorogenic acid and its related compounds on the invasion of hepatoma cells in culture. *Cytotechnology* **33**:229–235.

Yamagata K, Izawa Y, Onodera D, and Tagami M (2018) Chlorogenic acid regulates apoptosis and stem cell marker-related gene expression in A549 human lung cancer cells. *Mol Cell Biochem* **441**:9–19.
Yan Y, Liu N, Hou N, Dong L, and Li J (2017) Chlorogenic acid inhibits hepatocellular carcinoma in vitro and in vivo. *J Nutr Biochem* **46**:68–73.
Yang H, Said AM, Huang H, Papa APD, Jin G, Wu S, Ma N, Lan L, Shangguan F, and Zhang Q (2021) Chlorogenic acid depresses cellular bioenergetics to suppress pancreatic carcinoma through modulating c-Myc-TFR1 axis. *Phytother Res* **35**:2200–2210.
Yu JK, Yue CH, Pan YR, Chiu YW, Liu JY, Lin KI, and Lee CJ (2018) Isochlorogenic Acid C Reverses Epithelial-Mesenchymal Transition *via* Down-regulation of EGFR Pathway in MDA-MB-231 cells. *Anticancer Res* **38**:2127–2135.
Zeisberg M and Neilson EG (2009) Biomarkers for epithelial-mesenchymal transitions. *J Clin Invest* **119**:1429–1437.
Zhang J, Li Y, Liu Q, Lu W, and Bu G (2010) Wnt signaling activation and mammary gland hyperplasia in MMTV-LRP6 transgenic mice: implication for breast cancer tumorigenesis. *Oncogene* **29**:539–549.
Zhang JQ, Yao ZT, Liang GK, Chen X, Wu HH, Jin L, and Ding L (2015) [Combination of lapatinib with chlorogenic acid inhibits breast cancer metastasis by suppressing macrophage M2 polarization]. *Zhejiang Da Xue Xue Bao Yi Xue Ban* **44**:493–499.
Zhang M, Meng M, Liu Y, Qi J, Zhao Z, Qiao Y, Hu Y, Lu W, Zhou Z, Xu P, et al. (2021) Triptonide effectively inhibits triple-negative breast cancer metastasis through concurrent degradation of Twist1 and Notch1 oncoproteins. *Breast Cancer Res* **23**:116.

Address correspondence to: Professor Hongwei Guo, Guangxi Medical University, 22 Shuangyong Road, Nanning 530021, China. E-mail: hongweiguo@gxmu.edu.cn; Yiqiang Ouyang, Guangxi Medical University, 22 Shuangyong Road, Nanning 530021, China. E-mail: ouyangyiqiang@stu.gxmu.edu.cn; Qinpei Lu, Guangxi Medical University, 22 Shuangyong Road, Nanning 530021, China. E-mail: luqinpei@gxmu.edu.cn